High-precision absolute distance and vibration measurement with frequency scanned interferometry

Hai-Jun Yang, Jason Deibel, Sven Nyberg, and Keith Riles

We report high-precision absolute distance and vibration measurements performed with frequency scanned interferometry using a pair of single-mode optical fibers. Absolute distance was determined by counting the interference fringes produced while scanning the laser frequency. A high-finesse Fabry–Perot interferometer was used to determine frequency changes during scanning. Two multiple-distance-measurement analysis techniques were developed to improve distance precision and to extract the amplitude and frequency of vibrations. Under laboratory conditions, measurement precision of ~50 nm was achieved for absolute distances ranging from 0.1 to 0.7 m by use of the first multiple-distance-measurement technique. The second analysis technique has the capability to measure vibration frequencies ranging from 0.1 to 100 Hz with an amplitude as small as a few nanometers without *a priori* knowledge.

OCIS codes: 120.0120, 120.3180, 120.2650, 120.7280, 060.2430.

1. Introduction

The motivation for this project is to design a novel optical system for quasi-real-time alignment of tracker detector elements used in high-energy physics experiments. Fox-Murphy *et al.* from Oxford University reported their design of a frequency scanned interferometer (FSI) for precise alignment of the ATLAS Inner Detector.[1] Given the demonstrated need for improvements in detector performance, we plan to design an enhanced FSI system to be used for the alignment of tracker elements in the next generation of electron–positron linear collider detectors. Current plans for future detectors require a spatial resolution for signals from a tracker detector, such as a silicon microstrip or a silicon drift detector, to be approximately 7–10 μm.[2] To achieve this required spatial resolution, the measurement precision of absolute distance changes of tracker elements in one dimension should be of the order of 1 μm. Simultaneous measurements from hundreds of interferometers will be used to determine the three-dimensional positions of the tracker elements.

The authors are with the Department of Physics, University of Michigan, Ann Arbor, Michigan 48109-1120. H.-J. Yang's e-mail address is yhj@umich.edu.

Received 12 July 2004; revised manuscript received 24 November 2004; accepted 25 November 2004.

0003-6935/05/193937-08$15.00/0

We describe here a demonstration FSI system built in the laboratory for initial feasibility studies. The main goal was to determine the potential accuracy of absolute distance measurements (ADMs) that could be achieved under controlled conditions. Secondary goals included estimating the effects of vibrations and studying error sources crucial to the absolute distance accuracy. A significant amount of research on ADMs by use of wavelength-scanning interferometers already exists.[3–8] In one of the most comprehensive publications on this subject, Stone *et al.* describe in detail a wavelength-scanning heterodyne interferometer consisting of a system built around both a reference and a measurement interferometer[3]; the measurement precisions of absolute distance ranging from 0.3 to 5 m are ~250 nm by the averaging of distance measurements from 80 independent scans.

Detectors for high-energy physics experiment must usually be operated remotely for safety reasons because of intensive radiation, high voltage, or strong magnetic fields. In addition, precise tracking elements are typically surrounded by other detector components, making access difficult. For practical high-energy physics application of FSI, optical fibers for light delivery and return are therefore necessary.

We constructed a FSI demonstration system by employing a pair of single-mode optical fibers that are each approximately 1 m in length, one for transporting the laser beam to the beam splitter and retroreflector and another for receiving return beams. A key

issue for the optical fiber FSI is that the intensity of the return beams received by the optical fiber is very weak; the natural geometric efficiency is 6.25×10^{-10} for a measurement distance of 0.5 m. In our design, we use a gradient-index (GRIN) lens to collimate the output beam from the optical fiber.

We believe our work represents a significant advancement in the field of FSI in that high-precision ADMs and vibration measurements are performed (without *a priori* knowledge of vibration strengths and frequencies) using a tunable laser, an isolator, an off-the-shelf Fabry–Perot (F–P) interferometer, a fiber coupler, two single-mode optical fibers, an interferometer, and novel fringe analysis and vibration extraction techniques. Two new multiple-distance-measurement analysis techniques are used to improve precision and to extract the amplitude and frequency of vibrations. Expected dispersion effects when a corner cube prism or a beam-splitter substrate lies in the interferometer beam path are confirmed, and observed results agree well with results from numerical simulation. When present, the dispersion effect has a significant effect on the ADM. The limitations of our current FSI system are also discussed and major uncertainties are estimated.

2. Principles

The intensity I of any two-beam interferometer can be expressed as

$$I = I_1 + I_2 + 2\sqrt{I_1 I_2}\cos(\phi_1 - \phi_2), \tag{1}$$

where I_1 and I_2 are the intensities of the two combined beams and ϕ_1 and ϕ_2 are the phases. Assuming that the optical path lengths of the two beams are L_1 and L_2, the phase difference in Eq. (1) is $\Phi = \phi_1 - \phi_2 = 2\pi|L_1 - L_2|(\nu/c)$, where ν is the optical frequency of the laser beam and c is the speed of light.

For a fixed-path interferometer, as the frequency of the laser is continuously scanned, the optical beams will constructively and destructively interfere, causing fringes. The number of fringes ΔN is

$$\Delta N = |L_1 - L_2|(\Delta\nu/c) = L\Delta\nu/c, \tag{2}$$

where L is the optical path difference (OPD) between the two beams and $\Delta\nu$ is the scanned frequency range. The OPD (for absolute distance between the beam splitter and the retroreflector) can be determined by counting interference fringes while scanning the laser frequency.

3. Demonstration System of the Frequency Scanned Interferometer

A schematic of the FSI system with a pair of optical fibers is shown in Fig. 1. The light source is a New Focus Velocity 6308 tunable laser (665.1 nm $< \lambda <$ 675.2 nm). A high-finesse (>200) Thorlabs SA200 F–P is used to measure the frequency range scanned by the laser. The free spectral range of two adjacent F–P peaks is 1.5 GHz, which corresponds to

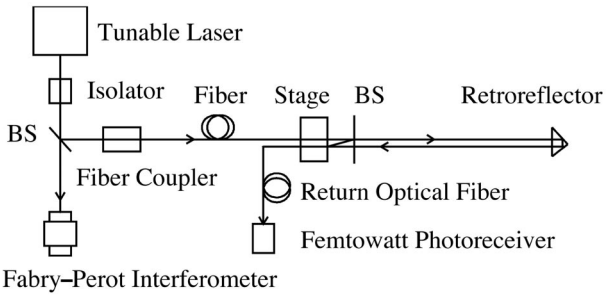

Fig. 1. Schematic of an optical fiber FSI system. BS, beam splitter.

0.002 nm. A Faraday isolator was used to reject light reflected back into the lasing cavity. The laser beam was coupled into a single-mode optical fiber with a fiber coupler. Data acquisition is based on a National Instruments data-acquisition card capable of simultaneously sampling four channels at a rate of 5 (MS/s)/channel (here MS means million samples) with a precision of 12 bits. Omega thermistors with a tolerance of 0.02 K and a precision of 0.01 mK are used to monitor the temperature. The apparatus is supported on a damped Newport optical table.

To reduce airflow and temperature fluctuations, a transparent plastic box was constructed on top of the optical table. Polyvinylchloride (PVC) pipes were installed to shield the volume of air surrounding the laser beam. Inside the PVC pipes, the typical standard deviation of 20 temperature measurements was $\approx$0.5 mK. Temperature fluctuations were suppressed by a factor of approximately 100 by employing the plastic box and PVC pipes.

The beam intensity coupled into the return optical fiber is very weak, requiring ultrasensitive photodetectors for detection. Considering the limited laser beam intensity and the need to split into many beams to serve a set of interferometers, it is vital to increase the geometric efficiency. To this end, a collimator is built by placing an optical fiber in a ferrule (1 mm in diameter) and gluing one end of the optical fiber to a GRIN lens. The GRIN lens is a 0.25 pitch lens with a 0.46 numerical aperture, 1 mm in diameter, and 2.58 mm in length that is optimized for a wavelength of 630 nm. The density of the outgoing beam from the optical fiber is increased by a factor of approximately 1000 by use of a GRIN lens. The return beams are received by another optical fiber and amplified by a silicon femtowatt photoreceiver with a gain of 2×10^{10} V/A.

4. Multiple-Distance-Measurement Techniques

For a FSI system, drifts and vibrations occurring along the optical path during the scan will be magnified by a factor of $\Omega = \nu/\Delta\nu$, where ν is the average optical frequency of the laser beam and $\Delta\nu$ is the scanned frequency. For the full scan of our laser, $\Omega \sim 67$. Small vibrations and drift errors that have negligible effects for many optical applications may have a significant effect on a FSI system. A single-

frequency vibration may be expressed as $x_{vib}(t) = a_{vib}\cos(2\pi f_{vib}t + \phi_{vib})$, where a_{vib}, f_{vib}, and ϕ_{vib} are the amplitude, frequency, and phase of the vibration, respectively. If t_0 is the start time of the scan, Eq. (2) can be rewritten as

$$\Delta N = L\Delta\nu/c + 2[x_{vib}(t)\nu(t) - x_{vib}(t_0)\nu(t_0)]/c. \quad (3)$$

If we approximate $\nu(t) \sim \nu(t_0) = \nu$, the measured OPD L_{meas} may be expressed as

$$L_{meas} = L_{true} - 4a_{vib}\Omega \sin[\pi f_{vib}(t - t_0)] \times \sin[\pi f_{vib}(t + t_0) + \phi_{vib}], \quad (4)$$

where L_{true} is the true OPD without vibration effects. If the path-averaged refractive index of ambient air $\bar{n}_g$ is known, the measured distance is $R_{meas} = L_{meas}/(2\bar{n}_g)$.

If the measurement window size $(t - t_0)$ is fixed and the window used to measure a set of R_{meas} is sequentially shifted, the effects of the vibration will be evident. We use a set of distance measurements in one scan by successively shifting the fixed-length measurement window one F–P peak forward each time. The arithmetic average of all measured R_{meas} values in one scan is taken to be the measured distance of the scan (although more sophisticated fitting methods can be used to extract the central value). For a large number of distance measurements N_{meas}, the vibration effects can be greatly suppressed. Of course statistical uncertainties from fringe and frequency determination, dominant in our current system, can also be reduced with multiple scans. Averaging multiple measurements in one scan, however, provides similar precision improvement as averaging distance measurements from independent scans and is faster, more efficient, and less susceptible to systematic errors from drift. In this way, we can improve the distance accuracy dramatically if there are no significant drift errors during one scan, caused, for example, by temperature variation. This multiple-distance-measurement technique is called slip measurement window with fixed size, shown in Fig. 2. However, there is a trade-off in that the thermal drift error is increased with the increase of N_{meas} because of the larger magnification factor Ω for a smaller measurement window size.

To extract the amplitude and frequency of the vibration, another multiple-distance-measurement technique called slip measurement window with fixed start point is shown in Fig. 2. In Eq. (3), if t_0 is fixed, the measurement window size is one enlarged F–P peak for each shift; an oscillation of a set of measured R_{meas} values reflects the amplitude and frequency of vibration. This technique is not suitable for distance measurement because there always exists an initial bias term including t_0 that cannot be determined accurately in our current system.

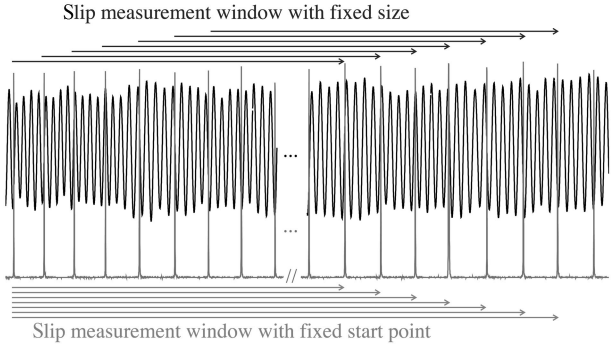

Fig. 2. Schematic of two multiple-distance-measurement techniques. The interference fringes from the femtowatt photoreceiver and the scanning frequency peaks from the F–P interferometer for the optical fiber FSI system recorded simultaneously by a data-acquisition card are shown as waves and sharp peaks, respectively. The free spectral range of two adjacent F–P peaks (1.5 GHz) provides a calibration of the scanned frequency range.

5. Absolute Distance Measurement

The typical measurement residual versus the distance measurement number in one scan by use of the above technique is shown in Fig. 3(a), where the scanning rate was 0.5 nm/s and the sampling rate was 125 ksamples/s. Measured distances minus their average value for ten sequential scans are plotted versus number of measurements (N_{meas}) per scan in Fig. 3(b). The standard deviations (rms) of distance measurements for ten sequential scans are plotted versus

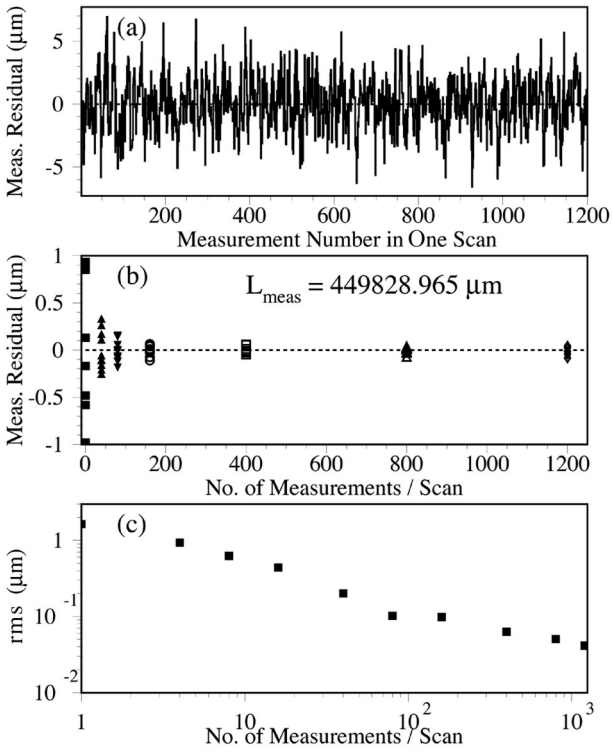

Fig. 3. Distance measurement residual spreads versus number of distance measurement N_{meas} (a) for one typical scan, (b) for ten sequential scans, (c) the standard deviation of distance measurements for ten sequential scans versus N_{meas}.

number of measurements (N_{meas}) per scan in Fig. 3(c). It can be seen that the distance errors decrease with an increase of N_{meas}. The rms of measured distances for ten sequential scans is 1.6 μm if there is only one distance measurement per scan ($N_{meas} = 1$). If $N_{meas} = 1200$ and the average value of 1200 distance measurements in each scan is considered as the final measured distance of the scan, the rms of the final measured distances for ten scans is 41 nm for the distance of 449828.965 μm; the relative distance measurement precision is 91 parts per billion (ppb).

Some typical measurement residuals are plotted versus the number of distance measurements in one scan (N_{meas}) for open-box and closed-box data with scanning rates of 2 and 0.5 nm/s in Figs. 4(a)–4(d), respectively. The measured distance is approximately 10.4 cm. It can be seen that the slow fluctuations of multiple distance measurements for open-box data are larger than that for closed-box data.

The standard deviation (rms) of measured distances for ten sequential scans is approximately 1.5 μm if there is only one distance measurement per scan for closed-box data. By use of the multiple-distance-measurement technique, the distance measurement precisions for various closed-box data with distances ranging from 10 to 70 cm collected in the past year are improved significantly. Precisions of approximately 63 nm are demonstrated under laboratory conditions, as shown in Table 1. All measured precisions listed in the Table 1 are the rms of measured distances for ten sequential scans. Two FSI demonstration systems, air FSI and optical fiber FSI, are constructed for extensive tests of the multiple-distance-measurement technique; air FSI means FSI with the laser beam transported entirely in the ambient atmosphere, and optical fiber FSI represents FSI with the laser beam delivered to the interferometer and received back by single-mode optical fibers.

On the basics of our studies, the slow fluctuations are reduced to a negligible level by using the plastic box and PVC pipes to suppress temperature fluctuations. The dominant error comes from the uncertainties of the interference fringes' number determination; the fringes' uncertainties are uncorrelated for multiple distance measurements. In this case, averaging multiple distance measurements in one scan provides a precision improvement similar to averaging distance measurements from multiple independent scans, but is faster, more efficient, and less susceptible to systematic errors from drift. However, for open-box data, the slow fluctuations are dominant, of the order of few micrometers in our laboratory. The measurement precisions for single- and multiple-distance open-box measurements are comparable, which indicates that the slow fluctuations cannot be adequately suppressed by using the multiple-distance measurement technique. A dual-laser FSI system[6,9] intended to cancel the drift error

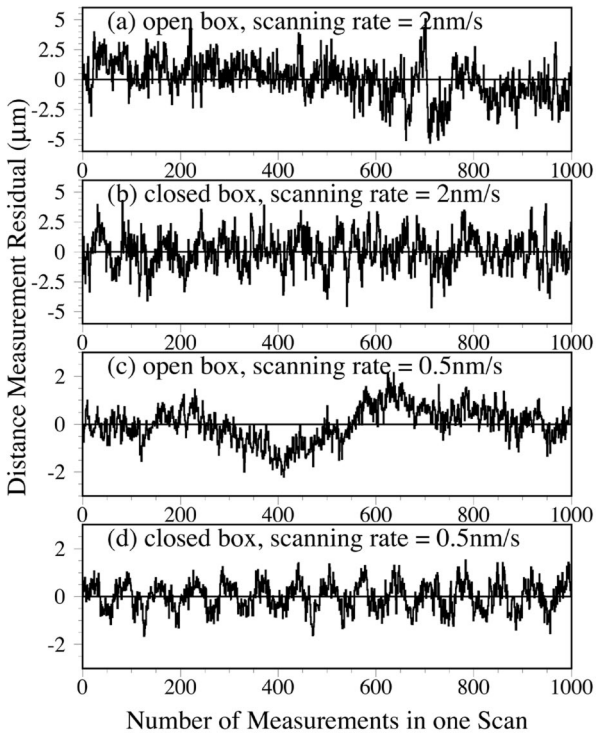

Fig. 4. Distance measurement residual spreads versus N_{meas} in one scan: (a) for the open box with a scanning rate of 2 nm/s, (b) for the closed box with a scanning rate of 2 nm/s, (c) for the open box with a scanning rate of 0.5 nm/s, (d) for the closed box with a scanning rate of 0.5 nm/s.

Table 1. Distance Measurement Precisions for Various Setups with the Multiple-Distance-Measurement Technique

Distance (cm)	Precision (μm)		Scanning Rate (nm/s)	FSI System
	Open Box	Closed Box		
10.385107	1.1	0.019	2.0	Optical fiber FSI
10.385105	1.0	0.035	0.5	Optical fiber FSI
20.555075	—	0.036, 0.032	0.8	Optical fiber FSI
20.555071	—	0.045, 0.028	0.4	Optical fiber FSI
41.025870	4.4	0.056, 0.053	0.4	Optical fiber FSI
44.982897	—	0.041	0.5	Optical fiber FSI
61.405952	—	0.051	0.25	Optical fiber FSI
65.557072	3.9, 4.7	—	0.5	Air FSI
70.645160	—	0.030, 0.034, 0.047	0.5	Air FSI

is currently under study in our laboratory (to be described in a subsequent paper).

From Fig. 4(d) we observe periodic oscillation of the distance measurement residuals in one scan, where the fitted frequency is 3.22 ± 0.01 Hz for the scan. The frequency depends on the scanning rate $f \sim$ (scanning rate in nm/s) × 60/(675.1 nm − 665.1 nm). From Eq. (4) it is clear that the amplitude of the vibration or oscillation pattern for multiple distance measurements depends on $4a_{\text{vib}}\Omega \sin[\pi f_{\text{vib}}(t - t_0)]$. If a_{vib} and f_{vib} are constant values, it depends on the size of the distance measurement window. Subsequent investigation with a CCD camera trained on the laser output revealed that the apparent ~3 Hz vibration during the 0.5 nm/s scan arose from the beam's centroid motion. Because the centroid motion is highly reproducible, we believe that the effect comes from motion of the internal hinged mirror in the laser used to scan its frequency.

The measurable distance range is limited in our current optical fiber FSI demonstration system for several reasons. For a given scanning rate of 0.25 nm/s, the produced interference fringes, estimated by $\Delta N \sim (2 \times \Delta L \times \Delta\nu)/c$, are approximately 26,400 in a 40 s scan for a measured distance (ΔL) of 60 cm, that is, ~660 fringes/s, where $\Delta\nu$ is the scanned frequency and c is the speed of light. The currently used femtowatt photoreceiver has a 3 dB frequency bandwidth ranging from 30 to 750 Hz; the transimpedance gain decreases quickly beyond 750 Hz. There are two ways to extend the measurable distance range. One straightforward way is to extend the effective frequency bandwidth of the femtowatt photoreceiver; the other way is to decrease the interference fringe rate by decreasing the laser scanning rate. There are two major drawbacks for the latter; one is that larger slow fluctuations occur during longer scanning times; the other is that the laser scanning is not stable enough to produce reliable interference fringes if the scanning rate is lower than 0.25 nm/s for our present tunable laser. In addition, another limitation to distance range is that the intensity of the return beam from the retroreflector decreases inverse quadratically with range.

6. Vibration Measurement

To test the vibration measurement technique, a piezoelectric transducer was employed to produce vibrations of the retroreflector. For example, the frequency of the controlled vibration source was set to 1.01 ± 0.01 Hz with an amplitude of 0.14 ± 0.02 μm. For $N_{\text{meas}} = 2000$ distance measurements in one scan, the magnification factor for each distance measurement depends on the scanned frequency of the measurement window, $\Omega(i) = \nu/\Delta\nu(i)$, where ν is the average frequency of the laser beam in the measurement window, and scanned frequency $\Delta\nu(i) = (4402 - N_{\text{meas}} + i) \times 1.5$ GHz, where i runs from 1 to N_{meas}, shown in Fig. 5(a). The distance measurement residuals for 2000 distance measurements in the scan are shown in Fig. 5(b); the oscillation of the measurement residuals reflect the vibration of the retroreflector. Since the vibration is magnified by a factor of $\Omega(i)$ for each distance measurement, the corrected measurement residuals are measurement residuals divided by the corresponding magnification factors, shown in Fig. 5(c). The extracted vibration frequencies and amplitudes that are used with this technique are $f_{\text{vib}} = 1.007 \pm 0.0001$ Hz and $A_{\text{vib}} = 0.138 \pm 0.0003$ μm, respectively, which is in good agreement with expectations.

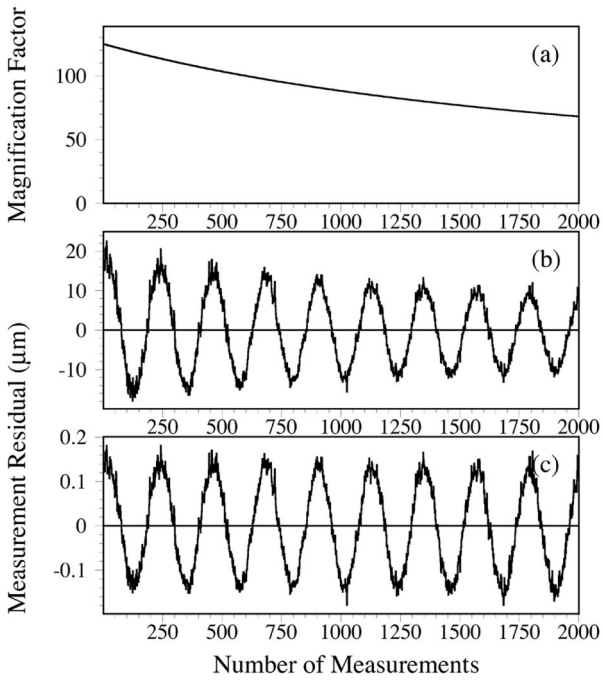

Fig. 5. Frequency and amplitude of the controlled vibration source are 1 Hz and 140 nm. (a) Magnification factor versus number of distance measurements, (b) distance measurement residual versus number of distance measurements, (c) corrected measurement residual versus number of distance measurements.

Another demonstration was made for the same vibration frequency, but with an amplitude of only 9.5 ± 1.5 nm. The magnification factors, distance measurement residuals, and corrected measurement residuals for 2000 measurements in one scan are shown in Figs. 6(a)–6(c), respectively. The extracted vibration frequencies and amplitudes used with this technique are $f_{\text{vib}} = 1.025 \pm 0.002$ Hz and $A_{\text{vib}} = 9.3 \pm 0.3$ nm.

In addition, vibration frequencies at 0.1, 0.5, 1.0, 5, 10, 20, 50, and 100 Hz with controlled vibration amplitudes ranging from 9.5 to 400 nm were studied extensively using our current FSI system. The measured vibrations and expected vibrations all agree well within the 10%–15% level for amplitudes, and 1%–2% for frequencies, where we are limited by uncertainties in the expectations. Vibration frequencies far below 0.1 Hz can be regarded as slow fluctuations, which cannot be suppressed by the above analysis techniques.

For comparison, nanometer vibration measurement by a self-aligned optical feedback vibrometry

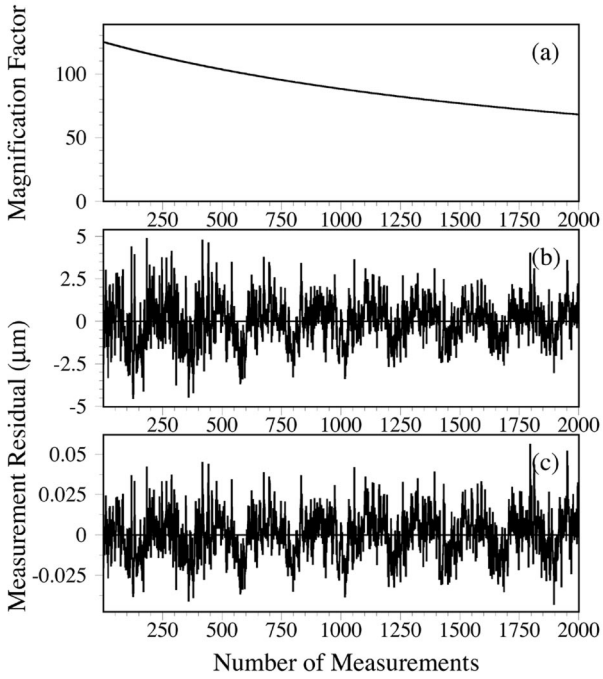

Fig. 6. Frequency and amplitude of the controlled vibration source are 1 Hz and 9.5 nm. (a) Magnification factor versus number of distance measurements, (b) distance measurement residual versus number of distance measurements, (c) corrected measurement residual versus number of distance measurements.

technique has been reported.[10] The vibrometry technique is able to measure vibration frequencies ranging from 20 Hz to 20 kHz with a minimal measurable vibration amplitude of 1 nm. Our second multiple-distance-measurement technique demonstrated above has the capability to measure vibration frequencies ranging from 0.1 to 100 Hz with minimal amplitude on the level of several nanometers, without *a priori* knowledge of the vibration strengths or frequencies.

7. Effect of Dispersion Effects on Distance Measurement

Dispersive elements such as a beam splitter or a corner cube prism in the interferometer can create an apparent offset in measured distance for a FSI system since the optical path length of the dispersive element changes during the scan. The small OPD change caused by dispersion is magnified by a factor of Ω and has a significant effect on the absolute distance measurement for the FSI system. The measured OPD difference L_{meas} can be expressed as

$$L_{\text{meas}} = |L(t)/\lambda(t) = L(t0)/\lambda(t0)|\, c/\Delta\nu,$$

$$L(t) = 2\{D1n_{\text{air}} + D2n[\lambda(t)]_{\text{corner cube}}\}, \qquad (5)$$

where $L(t)$ and $L(t0)$ refer to the OPD at times t and $t0$, respectively; $\lambda(t)$ and $\lambda(t0)$ are the wavelength of the laser beam at times t and $t0$; c is the speed of light; $D1$ and $D2$ are true geometric distances in the air and in the corner cube prism; and n_{air} and $n[\lambda(t)]_{\text{corner cube}}$ are the refractive index of ambient atmosphere and the refractive index of the corner cube prism for $\lambda(t)$, respectively. The measured distance $R_{\text{meas}} = L_{\text{meas}}/(2\bar{n}_g)$, where $\bar{n}_g$ is the average refractive index around the optical path.

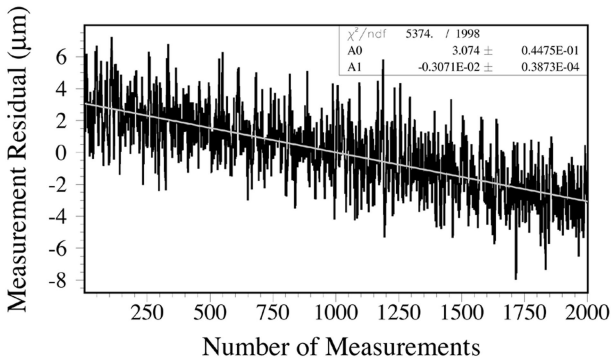

Fig. 7. Residuals of 2000 distance measurements for one typical scan; the corner cube prism is used as retroreflector.

The Sellmeier formula for dispersion in crown glass (BK-7)[11] can be written as

$$n^2(\lambda) = 1 + \frac{B_1\lambda^2}{\lambda^2 - C_1} + \frac{B_2\lambda^2}{\lambda^2 - C_2} + \frac{B_3\lambda^2}{\lambda^2 - C_3}, \qquad (6)$$

where the beam wavelength λ is in units of micrometers, $B_1 = 1.03961212$, $B_2 = 0.231792344$, $B_3 = 1.01046945$, $C_1 = 0.00600069867$, $C_2 = 0.0200179144$, and $C_3 = 103.560653$.

If we use the first multiple-distance-measurement technique described above to make 2000 distance measurements for one typical scan, where the corner cube prism is used as retroreflector, we observe a highly reproducible drift in measured distance, as shown in Fig. 7 where the fitted distance drift is 6.14 ± 0.08 μm for one typical scan with a straight-line fit. However, there is no apparent drift if we replace the corner cube prism by the hollow retroreflector.

Numerical simulations have been carried out using Eqs. (5) and (6) to understand the above phenomena. For example, consider the case $D1 = 20.97$ cm and $D2 = 1.86$ cm (the uncertainty of $D2$ is 0.06 cm), where the first and last measured distances among 2000 sequential distance measurements are denoted R_1 and R_{2000}, respectively. Using the Sellmeier equation [Eq. (6)] to model the corner cube prism material (BK-7) dispersion, we expect $R_1 - (D1 + D2) = 373.876$ μm and $R_{2000} - (D1 + D2) = 367.707$ μm. The difference between R_1 and R_{2000} is 6.2 ± 0.2 μm, which agrees well with our observed 6.14 ± 0.08 μm drift over 2000 measured distances. The measured distance shift and drift strongly depend on $D2$, but are insensitive to $D1$. A change of 1 cm in $D1$ leads to a 3 nm distance shift, but the same change in $D2$ leads to a 200 μm distance shift. If a beam splitter is oriented with its reflecting side

facing the laser beam, then there is an additional dispersive distance shift. We verified this effect with 1 and a 5 mm beam splitters. When we insert an additional beam splitter with 1 mm thickness between the retroreflector and the original beam splitter in the optical fiber FSI system, we observe a 500 μm shift on measured distance if n_g is fixed consistent with the numerical simulation result. For the 5 mm beam splitter (the measured thickness of the beam splitter is 4.6 ± 0.05 mm), the first 20 scans were performed with the beam splitter's antireflecting surface facing the optical fibers and the second 20 scans with the reflecting surface facing the optical fibers. The expected drifts ($R_{2000} - R_1$) for the first and the second 20 scans from the dispersion effect are 0 and −1.53 ± 0.05 μm, respectively. The measured drifts obtained by averaging the measurements from 20 sequential scans are −0.003 ± 0.12 μm and −1.35 ± 0.17 μm, respectively. The measured values agree well with expectations. In addition, the dispersion effect from air[12,13] is also estimated by using numerical simulation. The expected drift ($R_{2000} - R_1$) from air dispersion is approximately −0.07 μm for an optical path of 50cm in air; this effect cannot be detected for our current FSI system. However, it could be verified by using a FSI with a vacuum tube surrounding the laser beam; the measured distance with air in the tube would be approximately 4 μm larger than for an evacuated tube.

In summary, dispersion effects can have a significant effect on absolute distance measurements, but can be minimized with care for elements placed in the interferometer or corrected for once any necessary dispersive elements in the interferometer are understood.

8. Error Estimations

Some major error sources are estimated in the following:

(1) Error from uncertainties of fringe and scanned frequency determination. The measurement precision of the distance R (the error due to the air's refractive-index uncertainty is considered separately below) is given by $(\sigma_R/R)^2 = (\sigma_{\Delta N}/\Delta N)^2 + (\sigma_{\Delta\nu}/\Delta\nu)^2$, where R, ΔN, $\Delta\nu$, σ_R, $\sigma_{\Delta N}$, and $\sigma_{\Delta\nu}$ are measurement distance, fringe numbers, scanned frequency, and their corresponding errors. For a typical scanning rate of 0.5 nm/s with a 10 nm scan range, the full scan time is 20 s. The total number of samples for one scan is 2.5 MS at a sampling rate of 125 kS/s. There is an approximate 4–5 sample ambiguity in fringe peak and valley position due to a vanishing slope and the limitation of the 12 bit sampling precision. However, there is a much smaller uncertainty for the F–P peaks because of their sharpness. Thus the estimated uncertainty is $\sigma_R/R \sim 1.9$ parts per million (ppm) for one full scan for a magnification factor $\Omega = 67$. If the number of distance measurements $N_{\text{meas}} = 1200$, the distance measurement window is smaller and the corresponding magnification factor is $\Omega^* = \nu/\Delta\nu$, where ν is the average frequency of the laser beam, $\Delta\nu = (4402 - N_{\text{meas}}) \times 1.5$ GHz. One obtains $\Omega^* \sim 94$ and $\sigma_R/R \sim 1.9 \text{ ppm} \times \Omega^*/\Omega/\sqrt{N_{\text{meas}}} \sim 77$ ppb.

(2) Error from vibrations. The detected amplitude and frequency for vibration (without a controlled vibration source) are ≈0.3 μm and 3.2 Hz. The corresponding time for $N_{\text{meas}} = 1200$ sequential distance measurements is 5.3 s. A rough estimation of the resulting error gives $\sigma_R/R \sim 0.3\ \mu\text{m}/(5.3\text{ s} \times 3.2\text{ Hz} \times 4)/R \sim 10$ ppb for a given measured distance of $R = 0.45$ m.

(3) Error from thermal drift. The refractive index of air depends on air temperature, humidity, and pressure (fluctuations of humidity and pressure have negligible effects on distance measurements for the 20 s scan). Temperature fluctuations are well controlled down to ≈0.5 mK (rms) in our laboratory by the plastic box on the optical table and the pipe shielding the volume of air near the laser beam. For a room temperature of 21 °C, an air temperature change of 1 K will result in a 0.9 ppm change of air refractive index. For a temperature variation of 0.5 mK in the pipe, $N_{\text{meas}} = 1200$ distance measurements, the estimated error will be $\sigma_R/R \sim 0.9\text{ ppm}/K \times 0.5\text{ mK} \times \Omega^* \sim 42$ ppb, where the magnification factor $\Omega^* = 94$.

The total error from the above sources, when added in quadrature, is ~89 ppb, with the major error sources arising from the uncertainty of fringe determination and the thermal drift. The estimated relative error agrees well with measured relative spreads of 91 ppb in real data for a measured distance of ≈0.45 m.

In addition to the above error sources, other sources can contribute to systematic bias in the absolute differential distance measurement. The major systematic bias comes from the uncertainty in the free spectral range of the F–P used to determine the scanned frequency range. The relative error would be $\sigma_R/R \sim 50$ ppb if the FSR were calibrated by a wavemeter with a precision of 50 ppb. A wavemeter of this precision was not available for the measurements described here. The systematic bias from the multiple-distance-measurement technique was also estimated by changing the starting point of the measurement window, the window size, and the number of measurements; the uncertainties typically range from 10 to 50 nm. Systematic bias from uncertainties in temperature, air humidity, and barometric pressure scales are estimated to be negligible.

9. Conclusion

An optical fiber FSI system was constructed to make high-precision absolute distance and vibration measurements. A design of the optical fiber with a GRIN lens was presented that improves the geometric efficiency significantly. Two new multiple-distance-measurement analysis techniques were presented to improve distance precision and to extract the amplitude and frequency of vibrations. ADM precisions of approximately 50 nm for distances ranging from 10

to 70 cm under laboratory conditions were achieved using the first analysis technique. The second analysis technique measures vibration frequencies ranging from 0.1 to 100 Hz with a minimal amplitude of a few nanometers. We verified an expected dispersion effect and confirmed its importance when we placed dispersive elements in the interferometer. Major error sources were estimated, and the observed errors were found to be in good agreement with expectation.

This research is supported by the National Science Foundation and the U.S. Department of Energy.

References

1. A. F. Fox-Murphy, D. F. Howell, R. B. Nickerson, and A. R. Weidberg, "Frequency scanned interferometry (FSI): the basis of a survey system for ATLAS using fast automated remote interferometry," Nucl. Instrum. Methods A **383,** 229–237 (1996).
2. American Linear Collider Working Group, "Linear Collider Physics, Resource Book for Snowmass 2001," hep-ex/0106058, SLAC-R-570 299-423 (Stanford Linear Collider Center, Stanford University, 2001), pp. 299–423.
3. J. A. Stone, A. Stejskal, and L. Howard, "Absolute interferometry with a 670-nm external cavity diode laser," Appl. Opt. **38,** 5981–5994 (1999).
4. D. Xiaoli and S. Katuo, "High-accuracy absolute distance measurement by means of wavelength scanning heterodyne interferometry," Meas. Sci. Technol. **9,** 1031–1035 (1998).
5. G. P. Barwood, P. Gill, and W. R. C. Rowley, "High-accuracy length metrology using multiple-stage swept-frequency interferometry with laser diodes," Meas. Sci. Technol. **9,** 1036–1041 (1998).
6. K. H. Bechstein and W. Fuchs, "Absolute interferometric distance measurements applying a variable synthetic wavelength," J. Opt. **29,** 179–182 (1998).
7. J. Thiel, T. Pfeifer, and M. Haetmann, "Interferometric measurement of absolute distances of up to 40 m," Measurement **16,** 1–6 (1995).
8. H. Kikuta and R. Nagata, "Distance measurement by wavelength shift of laser diode light," Appl. Opt. **25,** 976–980 (1986).
9. P. A. Coe, "An investigation of frequency scanning interferometry for the alignment of the ATLAS semiconductor tracker," Ph.D. dissertation (St. Peter's College, University of Oxford, Oxford, UK, 2001).
10. K. Otsuka, K. Abe, J. Y. Ko, and T. S. Lim, "Real-time nanometer-vibration measurement with a self-mixing microchip solid-state laser," Opt. Lett. **27,** 1339–1341 (2002).
11. SCHOTT'96 for Windows Catalog Optical Glass (Schott Glaswerke Mainz, Germany, 1996), http://us.schott.com/sgt/english/products/catalogs.html.
12. E. R. Peck and K. Reeder, "Dispersion of air," J. Opt. Soc. Am. **62,** 958–962 (1972).
13. P. E. Ciddor, "Refractive index of air: new equations for the visible and near infrared," Appl. Opt. **35,** 1566–1573 (1996).